Lorentz transmission electron microscopy on NiFe/Cu/Co/NiFe/MnNi active spin valve elements

Cite as: Appl. Phys. Lett. **71**, 2032 (1997); https://doi.org/10.1063/1.119778 Submitted: 03 June 1997 . Accepted: 01 August 1997 . Published Online: 05 August 1998

X. Portier, A. K. Petford-Long, R. C. Doole, T. C. Anthony, and J. A. Brug





ARTICLES YOU MAY BE INTERESTED IN

Lorentz microscopy of circular ferromagnetic permalloy nanodisks Applied Physics Letters 77, 2909 (2000); https://doi.org/10.1063/1.1320465

Switching of nanoscale magnetic elements

Applied Physics Letters **75**, 3683 (1999); https://doi.org/10.1063/1.125428

Lorentz transmission electron microscope study of ferromagnetic domain walls in $SrRuO_3$: Statics, dynamics, and crystal structure correlation

Journal of Applied Physics 85, 4131 (1999); https://doi.org/10.1063/1.370322

Lock-in Amplifiers up to 600 MHz







Lorentz transmission electron microscopy on NiFe/Cu/Co/NiFe/MnNi active spin valve elements

X. Portier, a) A. K. Petford-Long, and R. C. Doole Department of Materials, University of Oxford, Oxford OX1 3PH, United Kingdom

T. C. Anthony and J. A. Brug

Hewlett-Packard Laboratories, Palo Alto, California, 94304

(Received 3 June 1997; accepted for publication 1 August 1997)

In situ magnetoresistance measurements on lithographically defined spin-valve elements were performed by means of Lorentz transmission electron microscopy. The observation of a magnetic domain structure and the simultaneous magnetoresistance measurement by applying controlled field and controlled current have led to a clear correlation between giant magnetoresistance and changes in the magnetic domain structure. A study of the spin-valve behavior with the increase of the applied current value is also shown. © 1997 American Institute of Physics. [S0003-6951(97)00540-8]

During the last decade, numerous studies have been devoted to spin-valve (SV) structures1 whose main feature is low-field giant magnetoresistive behavior.² SVs have thus received increasing attention recently for possible application as magnetoresistive read heads in magnetic storage systems. The magnetization direction (easy axis) of one of the magnetic layers (pinned layer) is fixed by an adjacent antiferromagnetic (AF) layer (pinning layer) through exchange coupling. The magnetization direction in the other magnetic layer (sense layer) can rotate by applying an external magnetic field. When the applied field is parallel to the easy axis, parallel (P) and anti-parallel (AP) configurations of the pinned and sense layers are created that correspond to the minimum and maximum resistance values, respectively. Among the techniques used to investigate the magnetic properties, Lorentz transmission electron microscopy (LTEM) enables the magnetic domain structure of such thin films to be observed³ and a number of advances in this technique has allowed a magnetic field to be applied to the film in situ in the microscope. Quantitative images corresponding to the projected magnetic induction of both ferromagnetic layers can be obtained⁴ but it has not been possible so far to observe active SV devices, namely, ones through which a current is being passed. Development of a new specimen holder, and of processes for fabricating active SV sensors on electron-transparent windows, has enabled both a controlled current and a controlled magnetic field to be applied to the simultaneously during magnetic observation.⁵ Improved understanding of the nucleation and propagation of magnetic domains in these structures is expected to lead to the fabrication of sensors less prone to magnetic domain noise.

We report, in this letter, results from studies of a $10 \ \mu m \times 10 \ \mu m$ SV element whose structure is NiFe/Cu/Co/NiFe/MnNi (8/3/2/6/25 nm). The use of MnNi (Ref. 6) as the AF pinning layer has been motivated by its better resistance to corrosion, larger exchange coupling strength, and higher thermal stability when compared to MnFe, the more common AF material used in SV structures. The influence of

The device configuration used is shown in cross section in Fig. 1(a), and consists of a 2 mm×2 mm Si wafer substrate with a SV element supported by a 40-nm-thick amorphous alumina layer. Details of the fabrication process are given elsewhere.⁵ The SV was deposited using dc magnetron sputtering. The SV and the Au pads can be clearly identified in the TEM image of a typical sample shown in Fig. 1(b). A controlled magnetic field from -400 to 400 Oe can be applied in the plane of the SV element. The SV is connected via Au-coated clamp pads to an electrical circuit which supplies an adjustable constant current and allows the voltage to be recorded. During the experiments, a fixed current is applied through the SV element and, by monitoring the change in voltage with change in applied field (H_a) , the magnetoresistance of the sample can be determined and a curve of the giant magnetoresistance (GMR) ratio (dR/R = (R $-R_{\rm sat}$) $/R_{\rm sat}$) against H_a can then be plotted. H_a was changed by 1 Oe every 10 s in order to reduce time dependent effects and was applied parallel to the easy axis. R_{sat} corresponds to the parallel state of the magnetic moments in

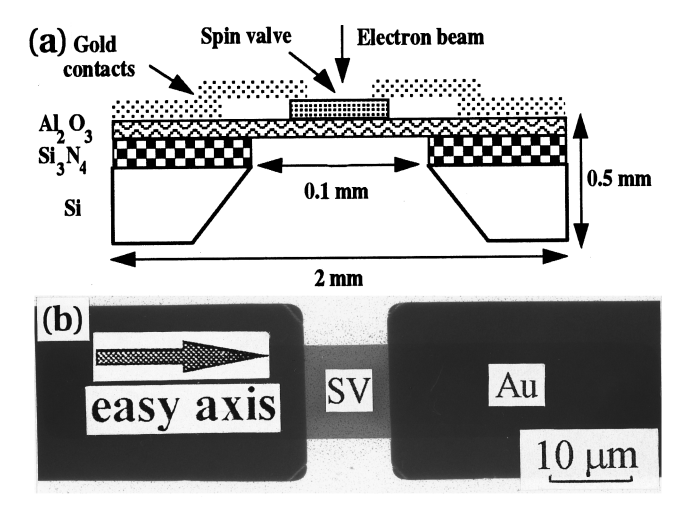


FIG. 1. (a) Cross-sectional view of the device which allows the *in situ* measurement of resistance in a Lorentz microscope, (b) TEM image of a $10~\mu\text{m}\times10~\mu\text{m}$ SV element with Au contacts at each end.

the applied current value on SV behavior has also been analyzed.

a)Electronic mail: xavier.portier@materials.ox.ac.uk

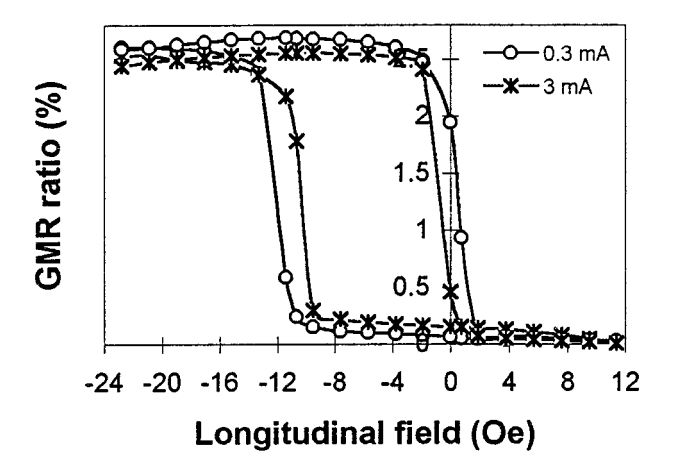


FIG. 2. Plot of the GMR ratio vs applied field parallel to the easy axis for current values of 0.3 and 3 mA. Slight decreases of the GMR ratio and coercivity are observed for the higher current value.

the ferromagnetic layers. Note that the lead resistance was not accounted for in this calculation, so the reported dR/R data are reduced from the value of 4.3% measured on the long test elements. Experiments were carried out for applied current values of 0.3 and 3 mA.

We made our observations using a modified JEOL 4000 EX TEM fitted with an AMG40 low-field objective lens pole piece (residual field at the sample is less than 1 G). The magnetic domain structure of the sample was observed in the Foucault mode of LTEM.³ The Foucault mode enables the domain shape and size, as well as the magnetization direction, to be determined from the domain contrast. The Foucault images have been formed by inserting an objective aperture to select the deflected beam corresponding to the parallel state of magnetization. Thus, the SV element appears white for the P state and black for the AP state. Assuming that the magnetization direction of the pinned layer is always parallel to the easy axis and in the same direction, each gray

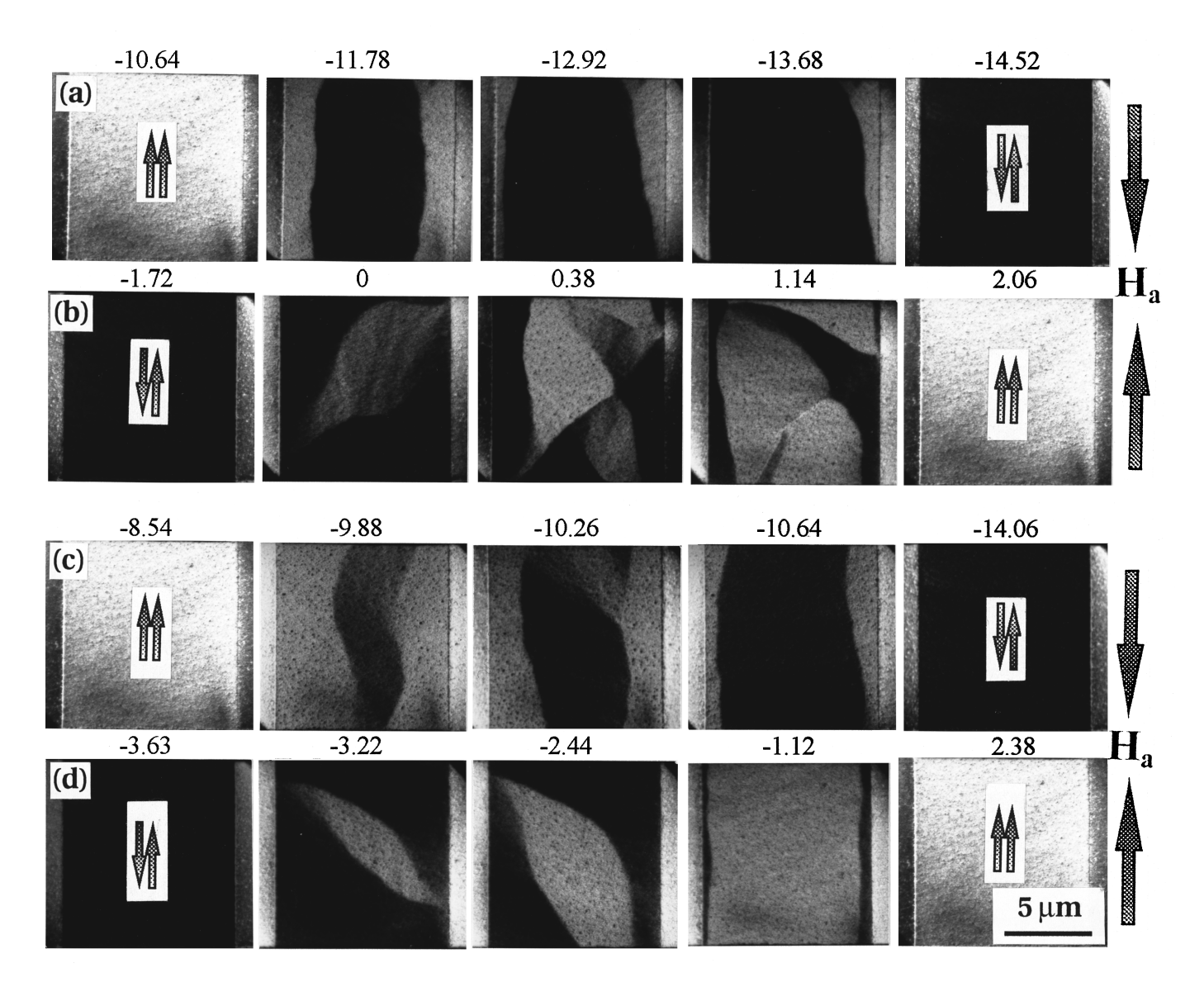


FIG. 3. Sets of Foucault images showing the change in domain shape and contrast of the SV element for applied current values of 0.3 mA (a) and (b) and 3 mA (c) and (d). The contacts are at the top and bottom of the images and the easy axis is pointing up vertically. The corresponding applied field value in Oe is indicated above each image.

level can be associated with a different magnetization direction of the sense layer.

Figure 2 shows plots of the GMR ratio versus H_a for applied current values of 0.3 and 3 mA. The asymmetry with respect to the origin is due to ferromagnetic coupling between the magnetic layers due to the so-called "orange peel" magnetostatic effect proposed by Néel, that results from roughness and waviness of the nonmagnetic and magnetic layers. The corresponding $R_{\rm sat}$ values are 28.7 and 31.8 Ω for 0.3 and 3 mA, respectively. With increasing current, a decrease of the GMR ratio is clearly seen from 2.7% to 2.5% and the coercivity is reduced from 13.0 to 9.9 Oe. These results are most probably due to an increase in temperature in the sense layer caused by the higher current density. Assuming that the thickness of conducting materials corresponds to the stacking of the pinned, spacer, and sense layers (~20 nm), the current densities for 0.3 and 3 mA are 1.5 $\times 10^5$ and 1.5×10^6 A cm⁻², respectively. The higher of these current densities is still more than an order of magnitude less than that used in actual SV recording heads.⁷

Figure 3 shows sets of Foucault images recorded simultaneously with the GMR curves seen in Fig. 2, allowing a direct correlation between magnetoresistance and domain structure to be made. Figures 3(a) and 3(b) show the changes for an applied current value of 0.3 mA. Figure 3(a) shows the P-AP magnetization reversal of the sense layer. The ferromagnetic coupling between the pinned and sense layers prevents any moment rotation in the sense layer away from the P direction until a field value at which sudden domain wall motion occurs and the sense layer magnetization flips to the AP configuration. The AP-P reversal of the sense layer, shown in Fig. 3(b), proceeds via moment rotation leading to the nucleation of a more complicated domain structure, as indicated by the presence of several gray levels in the image. Moment rotation occurs as the domain structure relaxes back to FM alignment of the pinned and sense layers. Figures 3(c) and 3(d) show the corresponding magnetization reversals of the sense layer for an applied current of 3 mA. In this case, the thermal energy supplied by the higher current density acts to partly overcome the effective FM coupling between the sense and pinned layers and also microstructural pinning of the magnetic moments. Both reversal processes of the sense layer then involve some moment rotation followed by nucleation and rapid motion of a simpler domain structure than that seen for 0.3 mA. The reversal mechanisms seen in Fig. 3 explain the shape of the GMR curves seen in Fig. 2. For all the reversal processes seen in Fig. 3, it is apparent that the edges of the SV element are the last to reverse their magnetization, showing the importance of edge effects induced by the lithographic definition of the element. Note that the field values at which the final image in each series was recorded are not necessarily those at which complete reversal of the sense layer is first observed.

The current density limit $(4.5 \times 10^6 \text{ A cm}^{-2})$, above which the film resistance increases dramatically has been reached for a current value of 9 mA. Figures 4(a) and 4(b) show Foucault images of the element "burned" in its midsection for H_a values of -0.76 and 3.54 Oe (AP-P transition), respectively. The presence of small domains with a complex distribution over this range of H_a values implies a

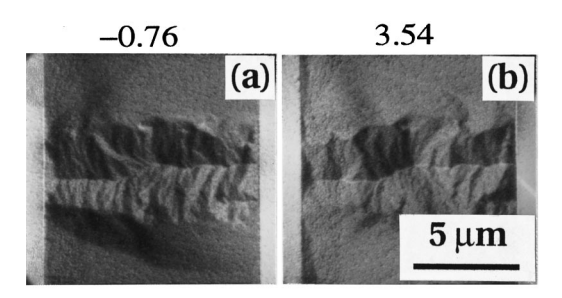


FIG. 4. Foucault images of a 10 μ m \times 10 μ m SV element whose middle part has been damaged by heating effects resulting from current values higher than 9 mA. The SV is not totally in the (a) AP or (b) in P state because of the small domains in the damaged region.

slower reversal mechanism in the damaged region, most likely as a result of a local modification in structure of the SV. Clearly, resistive heating can be quite significant even at low current density because of the lack of a heat sink beneath the device and the poor lateral heat conduction through the film itself.⁸

In conclusion, we have successfully observed active SV elements by means of LTEM. We have clearly shown that a change in the magnetic domain structure (domain size, shape, or contrast) corresponds to a change in resistance. An increase of the current density induces a decrease of the GMR ratio, and reduces the coercivity and the domain density of the sense layer. These features are explained by an increase in thermal energy induced by the higher current density.

Quantitative maps of the magnetic induction in the small SV element, extracted from the sum of a series of Foucault images, enable us to determine the magnetization direction of each domain in the sense layer. We believe that a direct estimate of the resistance can be deduced using Dieny's model which relates the angle between the easy axis and the magnetization direction of the domains.⁹ This study is now in progress.

This research was supported by Hewlett-Packard Laboratories in Palo Alto through a collaboration with the Department of Materials at Oxford University. The authors thank B. Garcia for fabrication of the lithographic masks. One of the authors (A.K.P.L.) thanks the Royal Society for financial support.

¹B. Dieny, V. S. Speriosu, S. Metin, S. S. P. Parkin, B. A. Gurney, P. Baumgart, and D. R. Wilhoit, J. Appl. Phys. **69**, 4771 (1991).

²M. Baibich, J. Broto, A. Fert, F. Nguyen Van Dau, F. Petroff, P. Etienne, G. Creuset, A. Friederich, and J. Chazelas, Phys. Rev. Lett. 61, 2472 (1988).

³J. P. Jakubovics, *Electron Microscopy in Materials Science*, edited by E. Ruedl and U. Valdre (Commission of the European Communities, Brussels, 1975), Vol. IV, p. 1303.

⁴M. F. Gillies, J. N. Chapman, and J. C. S. Kools, J. Appl. Phys. **78**, 5554 (1995).

⁵ X. Portier, A. K. Petford-Long, R. C. Doole, J. A. Brug, and T. C. Anthony, IEEE Trans. Magn. (in press).

⁶T. Lin, D. Mauri, N. Staud, C. Hwang, J. K. Howard, and G. L. Gorman, Appl. Phys. Lett. **65**, 1183 (1994).

⁷C. Tsang, R. E. Fontana, T. Lin, D. E. Heim, V. S. Speriosu, B. A. Gurney, and M. L. Williams, IEEE Trans. Magn. **30**, 3801 (1994).

⁸N. Ishiwata, T. Ishi, H. Matsutera, and K. Yamada, IEEE Trans. Magn. 32, 38 (1996).

⁹B. Dieny, J. Magn. Magn. Mater. **36**, 335 (1994).